



1 **Interactions of organosulfates with water vapor under sub- and supersaturated**  
2 **conditions**

3

4 Chao Peng,<sup>1,2</sup> Patricia N. Razafindrambinina,<sup>3</sup> Kotiba A. Malek,<sup>4</sup> Lanxiadi Chen,<sup>1,2,7</sup> Weigang  
5 Wang,<sup>5</sup> Ru-Jin Huang,<sup>6</sup> Yuqing Zhang,<sup>1,2</sup> Xiang Ding,<sup>1,2</sup> Maofa Ge,<sup>5</sup> Xinming Wang,<sup>1,2</sup> Akua A.  
6 Asa-Awuku,<sup>3,4</sup> and Mingjin Tang<sup>1,2,7,\*</sup>

7

8 <sup>1</sup> State Key Laboratory of Organic Geochemistry, Guangdong Key Laboratory of Environmental  
9 Protection and Resources Utilization, and Guangdong-Hong Kong-Macao Joint Laboratory for  
10 Environmental Pollution and Control, Guangzhou Institute of Geochemistry, Chinese Academy of  
11 Sciences, Guangzhou 510640, China

12 <sup>2</sup> CAS Center for Excellence in Deep Earth Science, Guangzhou 510640, China

13 <sup>3</sup> Department of Chemistry and Biochemistry, College of Computer, Mathematical and Natural  
14 Sciences, University of Maryland, College Park, MD 20742, USA

15 <sup>4</sup> Department of Chemical and Biomolecular Engineering, A. James Clark School of Engineering,  
16 University of Maryland, College Park, MD 20742, USA

17 <sup>5</sup> State Key Laboratory for Structural Chemistry of Unstable and Stable Species, Beijing National  
18 Laboratory for Molecular Sciences, CAS Research/Education Center for Excellence in Molecular  
19 Sciences, Institute of Chemistry, Chinese Academy of Sciences, Beijing 100190, China

20 <sup>6</sup> Key Laboratory of Aerosol Chemistry and Physics, State Key Laboratory of Loess and  
21 Quaternary Geology, Institute of Earth and Environment, Chinese Academy of Sciences, Xi'an  
22 710061, China



23 <sup>7</sup> University of Chinese Academy of Sciences, Beijing 100049, China

24

25 \*Correspondence: Mingjin Tang ([mingjintang@gig.ac.cn](mailto:mingjintang@gig.ac.cn))

26



27 **Abstract**

28 Organosulfates (OS) are important constituents of secondary organic aerosols, but their  
29 hygroscopic properties and cloud condensation nucleation (CCN) activities have not been well  
30 understood. In this work we employed three complementary techniques to characterize interactions  
31 of several OS with water vapor under sub- and supersaturated conditions. A vapor sorption  
32 analyzer was used to measure mass changes of OS samples with RH (0-90%); among the 11  
33 organosulfates examined, only sodium methyl sulfate (methyl-OS), sodium ethyl sulfate (ethyl-  
34 OS), sodium octyl sulfate (octyl-OS) and potassium hydroxyacetone sulfate were found to  
35 deliquesce as RH increased, and their mass growth factors at 90% RH were determined to be  
36  $3.652 \pm 0.064$ ,  $3.575 \pm 0.024$ ,  $1.591 \pm 0.004$  and  $2.202 \pm 0.031$ . Hygroscopic growth of methyl-, ethyl-  
37 and octyl-OS aerosols was also studied using a humidity tandem differential mobility analyzer (H-  
38 TDMA); continuous hygroscopic growth was observed, and their growth factors at 90% RH were  
39 determined to be  $1.83 \pm 0.03$ ,  $1.79 \pm 0.02$  and  $1.21 \pm 0.02$ . We further investigated CCN activities of  
40 methyl-, ethyl- and octyl-OS aerosols, and their single hygroscopicity parameters ( $\kappa_{\text{ccn}}$ ) were  
41 determined to be  $0.459 \pm 0.021$ ,  $0.397 \pm 0.010$  and  $0.206 \pm 0.008$ . For methyl- and ethyl-OS aerosols,  
42  $\kappa_{\text{ccn}}$  values agree reasonably well with those derived from H-TDMA measurements ( $\kappa_{\text{gf}}$ ), whereas  
43  $\kappa_{\text{ccn}}$  was found to be significantly larger than  $\kappa_{\text{gf}}$  for octyl-OS, likely due to both solubility limit  
44 and surface tension reduction.

45



## 46 **1 Introduction**

47 Secondary organic aerosol (SOA) contributes approximately 70% to the global atmospheric  
48 organic aerosols (Hallquist et al., 2009; Jimenez et al., 2009). SOA can affect the Earth's radiative  
49 forcing and climate directly by scattering and absorbing solar and terrestrial radiation, and also  
50 indirectly by acting as cloud condensation nuclei (CCN) or ice nucleating particles (Moise et al.,  
51 2015; Shrivastava et al., 2017). Consequently, it is important to understand the source, formation  
52 and physicochemical properties of SOA (Pöschl, 2005; Jimenez et al., 2009; Noziere et al., 2015).  
53 However, SOA concentrations on the global scale are significantly underestimated by many  
54 modeling studies (Heald et al., 2005; Kanakidou et al., 2005; Ervens et al., 2011; McNeill et al.,  
55 2012; Shrivastava et al., 2017), indicating that there might exist unknown while important  
56 precursors and/or formation mechanisms of SOA.

57 Organosulfates (OS), which could contribute to the total mass of ambient organic aerosols by  
58 as much as 30%, may largely explain the discrepancy between observed and modeled global SOA  
59 budgets (Surratt et al., 2008; Tolocka and Turpin, 2012; Liao et al., 2015). A number of field  
60 measurements have observed significant amounts of OS in ambient aerosols in different regions  
61 over the globe (Froyd et al., 2010; Kristensen and Glasius, 2011; He et al., 2014; Hettiyadura et  
62 al., 2015; Riva et al., 2019; Wang et al., 2019a; Wang et al., 2019b; Zhang et al., 2019;  
63 Brüggemann et al., 2020; Wang et al., 2020). For example, the mass concentration of sodium  
64 methyl sulfate, the smallest organosulfate, was found to be 0.2-9.3 ng m<sup>-3</sup> in Centreville, Alabama  
65 (Hettiyadura et al., 2017). Hydroxyacetone sulfate, which may originate from both biogenic  
66 (Surratt et al., 2008) and anthropogenic emissions (Hansen et al., 2014), has been detected at  
67 various locations, such as the Arctic (1.27-9.56 ng m<sup>-3</sup>) (Hansen et al., 2014), Beijing (0.5-7.5 ng  
68 m<sup>-3</sup>) (Wang et al., 2018), Xi'an (0.9-2.6 ng m<sup>-3</sup>) (Huang et al., 2018), Centreville (1.5-14.3 ng m<sup>-3</sup>)



69 (Hettiyadura et al., 2017) and Iowa City ( $4.8 \pm 1.1 \text{ ng m}^{-3}$ ) (Hughes and Stone, 2019). In addition,  
70 benzyl and phenyl sulfates were also ubiquitous in the troposphere, with reported concentrations  
71 up to almost  $1 \text{ ng m}^{-3}$  (Kundu et al., 2013; Ma et al., 2014; Staudt et al., 2014; Huang et al., 2018).

72 As OS are ubiquitous and abundant in the troposphere, it is important to understand their  
73 hygroscopic properties and CCN activities in order to assess their environmental and climatic  
74 effects (Kanakidou et al., 2005; Moise et al., 2015; Tang et al., 2016; Tang et al., 2019a). However,  
75 to our knowledge, only two previous studies have explored their hygroscopic properties and CCN  
76 activities (Hansen et al., 2015; Estillore et al., 2016). Hansen et al. (2015) investigated hygroscopic  
77 growth and CCN activation of limonene-derived OS (with molecular weight of 250 Da) and their  
78 mixtures with ammonium sulfate. Hygroscopicity of pure limonene-derived OS was weak, and its  
79 hygroscopic growth factors were determined to be 1.0 at 80% RH and 1.2 at 93% RH (Hansen et  
80 al., 2015). Estillore et al. (2016) investigated hygroscopic growth of a series of OS, including  
81 potassium salts of glycolic acid sulfate, hydroxyacetone sulfate, 4-hydroxy-2,3-epoxybutane  
82 sulfate, and 2-butenediol sulfate, as well as sodium salts of benzyl sulfate, methyl sulfate, ethyl  
83 sulfate, and propyl sulfate. Continuous hygroscopic growth (i.e. without obvious deliquescence)  
84 was observed for these OS aerosols (Estillore et al., 2016); in addition, their hygroscopic growth  
85 factors at 85% RH were determined to vary between 1.29 and 1.50, suggesting that their  
86 hygroscopicity showed substantial variation. In summary, it is fair to state that hygroscopic  
87 properties and CCN activities of OS have not been well understood.

88 In this work, three complementary techniques were used to investigate hygroscopic properties  
89 and CCN activities of a series of OS, including sodium methyl sulfate, sodium ethyl sulfate,  
90 sodium octyl sulfate, sodium dodecyl sulfate, potassium hydroxyacetone sulfate, potassium 3-  
91 hydroxy phenyl sulfate, potassium benzyl sulfate, potassium 2-methyl benzyl sulfate, potassium

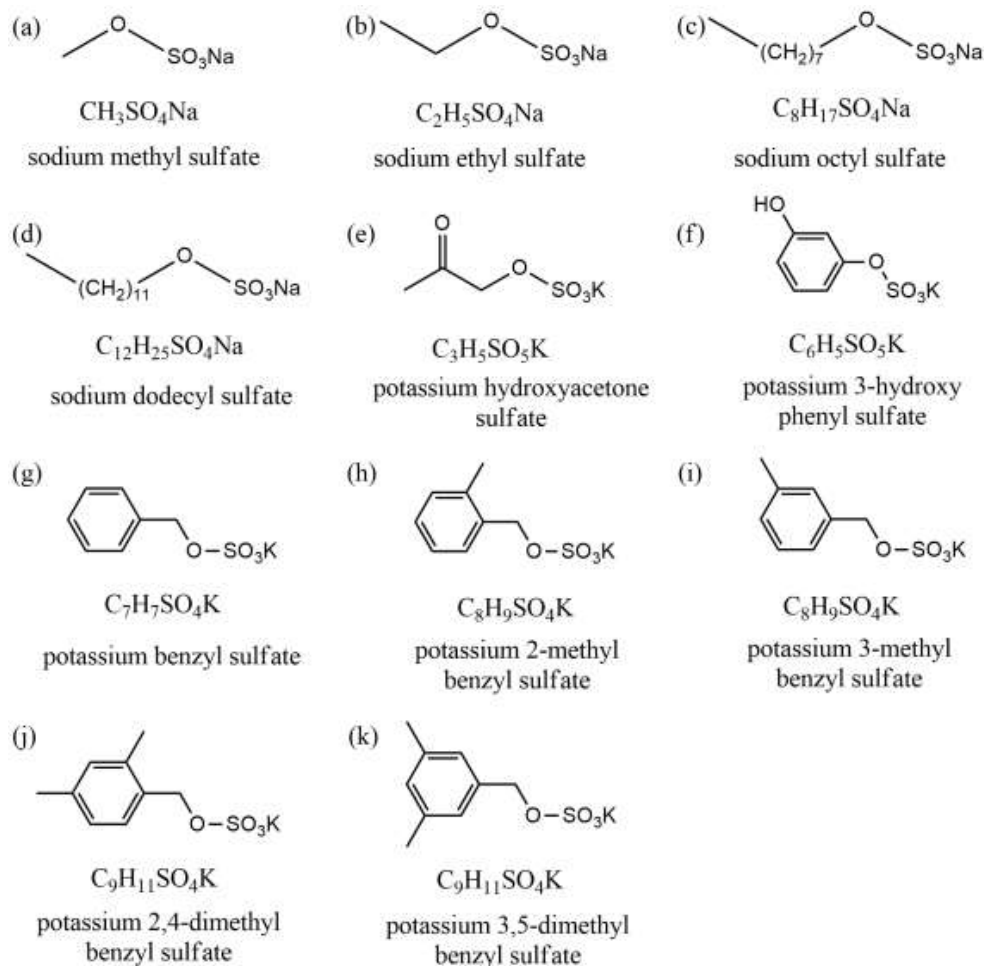


92 3-methyl benzyl sulfate, potassium 2,4-dimethyl benzyl sulfate and potassium 3,5-dimethyl benzyl  
93 sulfate. A vapor sorption analyzer was employed to measure mass change of these OS samples as  
94 a function of RH. In addition, hygroscopic growth (change in mobility diameters) and CCN  
95 activation of submicron aerosol particles were studied for sodium methyl sulfate, sodium ethyl  
96 sulfate and sodium octyl sulfate, using a humidity tandem differential mobility analyzer (H-TDMA)  
97 and a cloud condensation nuclei counter (CCNc). Due to their very limited quantities, we could  
98 not carry out H-TDMA and CCNc measurements for other OS samples which were synthesized  
99 by us. In addition, we also investigated the impacts of sodium methyl sulfate, sodium ethyl sulfate  
100 and sodium octyl sulfate on hygroscopic properties and CCN activities of ammonium sulfate.

## 101 **2 Experimental section**

### 102 **2.1 Chemicals and reagents**

103 Sodium methyl sulfate ( $\text{CH}_3\text{SO}_4\text{Na}$ , >98%) and sodium ethyl sulfate ( $\text{C}_2\text{H}_5\text{SO}_4\text{Na}$ , >98%)  
104 were purchased from Tokyo Chemical Industry (TCI); sodium octyl sulfate ( $\text{C}_8\text{H}_{17}\text{SO}_4\text{Na}$ , >99%),  
105 sodium dodecyl sulfate ( $\text{C}_{12}\text{H}_{25}\text{SO}_4\text{Na}$ , >99%) and ammonium sulfate (>99.5%) were supplied by  
106 Aldrich. The other seven OS, including potassium hydroxyacetone sulfate, potassium 3-hydroxy  
107 phenyl sulfate, potassium benzyl sulfate, potassium 2-methyl benzyl sulfate, potassium 3-methyl  
108 benzyl sulfate, potassium 2,4-dimethyl benzyl sulfate and potassium 3,5-dimethyl benzyl sulfate,  
109 were synthesized using the method described by Huang et al. (2018), and their purities were found  
110 to be >95% using nuclear magnetic resonance analysis. Chemical formulas and molecular  
111 structures of OS investigated in this study can be found in Figure 1.



112

113 **Figure 1.** Chemical formulas and molecular structures of organosulfates investigated in this study.

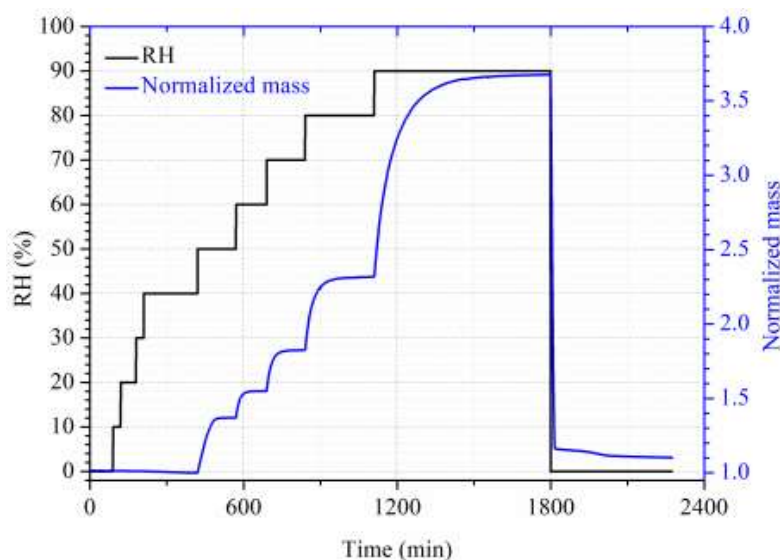
114

## 115 2.2 VSA experiments

116 A vapor sorption analyzer (VSA), commercialized by TA Instruments (New Castle, DE,  
117 USA), was used to measure mass change of organosulfates as a function of RH. Experimental  
118 details can be found in our previous studies (Chen et al., 2019; Gu et al., 2017; Guo et al., 2019;  
119 Tang et al., 2019b), and are thus described here briefly. Experiments were conducted at  $25 \pm 0.1$  °C



120 and in the RH range of 0-90%. A high precision balance was used to measure the sample mass at  
121 different RH with a stated sensitivity of  $<0.1 \mu\text{g}$ , and the dry mass of samples used in this work  
122 was typically around 1.0 mg.



123  
124 **Figure 2.** Change in RH (black curve, left y axis) and normalized sample mass (blue curve, right  
125 y axis) of  $\text{CH}_3\text{SO}_4\text{Na}$  with of time in a typical vapor sorption analyzer experiment at 25 °C.

126  
127 As shown in Figure 2, the mass of OS samples at different RH was determined by the VSA  
128 using the following method. RH was set to  $<1\%$  to dry the sample; after the sample mass was  
129 stabilized, RH was increased to 90% stepwise with an interval of 10% per step; at the end, RH was  
130 changed back to  $<1\%$  to dry the sample again. The sample was considered to reach the equilibrium  
131 at a given RH when the mass change was measured to be  $<0.1\%$  within 30 min. All the experiments  
132 were conducted at least three times in our work. The sample mass at a given RH ( $m$ ) was  
133 normalized to that at  $<1\%$  RH ( $m_0$ ) to determine the mass growth factor, defined as  $m/m_0$ .





### 134 **2.3 H-TDMA experiments**

135 A custom-built hygroscopicity tandem differential mobility analyzer (H-TDMA) was used to  
136 measure the mobility diameters of OS aerosol particles at different RH (5-90%) at  $24 \pm 1$  °C. The  
137 instrument was detailed elsewhere (Jing et al., 2016; Peng et al., 2016), and therefore only a brief  
138 introduction is given here. A commercial atomizer (MSP 1500) was used to produced polydisperse  
139 aerosol particles from dilute OS solutions in water (around 0.1 wt %), and the generated aerosol  
140 was dried to <5% RH by passing the aerosol flow through a Nafion dryer (MD-110-12S) and then  
141 a silica gel diffusion dryer. The dry aerosol flow was subsequently split to two flows. One aerosol  
142 flow was sent to the vent, and the other aerosol flow ( $0.3 \text{ L min}^{-1}$ ) was passed through the first  
143 differential mobility analyzer (DMA) to produce quasi-monodisperse aerosol particles with a  
144 mobility diameter of 100 nm. After that, the aerosol flow was humidified to a desired RH by  
145 flowing through a humidification section, which was made of two Nafion tubes (MD-700-12F-1)  
146 connected in series, and the residence time in the humidification section was  $\sim 27$  s. Finally, the  
147 size distribution of humidified aerosol was measured by a scanning mobility particle sizer (SMPS),  
148 which consisted of the second DMA coupled to a condensation particle counter (CPC 3776, TSI).  
149 RH of the aerosol flow and the sheath flow in the second DMA were maintained to be equal and  
150 monitored using a commercial dew-point hygrometer (Michell, UK) with a stated uncertainty of  
151  $\pm 0.08\%$  RH. In addition, the flow rate ratio of the sheath flow to the aerosol flow was set to 10:1  
152 for both DMAs.

153 Hygroscopic growth factors (GF), defined as  $d/d_0$  ( $d$  is the mobility diameter at a given RH  
154 and  $d_0$  is the mobility diameter at RH <5%) were reported. All the experiments were conducted in  
155 triplicate. During our experiments, ammonium sulfate was used to calibrate the H-TDMA system



156 routinely, and the absolute differences between the measured and theoretical GF at 90% RH were  
157 found to be within 0.04, confirming the robustness of our measurements.

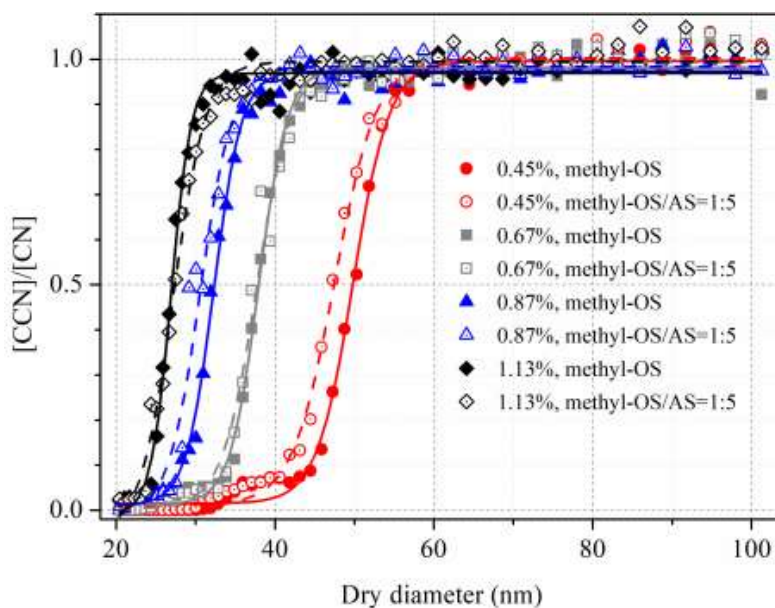
#### 158 **2.4 CCN experiments**

159 The CCN activity of aerosol particles was determined using a commercial cloud condensation  
160 nuclei counter (CCNc, CCN-100, Droplet Measurement Technologies, Longmont, CO, USA)  
161 described in previous studies (Roberts and Nenes, 2005; Lance et al., 2006; Moore et al., 2010).  
162 Polydisperse aerosol particles were generated using a commercial atomizer (TSI 3076), in which  
163 concentrations of solutions used were around 0.1 g/L. The wet aerosol flow generated was passed  
164 through two silica gel diffusion dryers to reduce its RH to <5% RH. After that, a dry aerosol flow  
165 (~800 mL min<sup>-1</sup>) was passed through a DMA (TSI 3081) in size scanning mode to produce quasi-  
166 monodisperse aerosols, and subsequently the aerosol flow was split to two streams: one stream  
167 (~300 mL/min) was sampled into a commercial CPC (TSI 3775) to measure total number  
168 concentrations of aerosol particles ([CN]), and the second flow (~500 mL/min) was sampled into  
169 the cloud condensation nuclei counter (CCNc, CCN-100) to measure number concentrations of  
170 CCN ([CCN]).

171 Activation fractions ([CCN]/[CN]) of size-resolved dry particles were determined using the  
172 Scanning Mobility CCN Analysis (SMCA) method described elsewhere (Moore et al., 2010). In  
173 brief, the DMA was operated in the scanning voltage mode, and thus one activation curve  
174 (activation fractions as a function of dry diameter) could be obtained in 60-120s. The multiple  
175 charge effect was also corrected in this method, and in our work the supersaturation (*SS*) was set  
176 in the range of 0.45-1.13% with the stated uncertainty to be ±0.01%. As shown in Figure 3,  
177 activation fractions of sodium methyl sulfate (methyl-OS) and its internally mixed aerosol with  
178 ammonium sulfate were measured at four different *SS* with dry mobility diameters between 20



179 and 100 nm. Activation fractions were fitted versus dry diameters, and the critical particle diameter  
180 ( $d_{50}$ ) was determined as the dry diameter at which the activation fraction is equal to 0.5. During  
181 our measurements, ammonium sulfate was used to calibrate supersaturations, and the Pitzer-ion  
182 interaction model was applied in the calibration procedure to account for incomplete dissociation  
183 of ammonium sulfate at droplet activation (Pitzer and Mayorga, 1973; Clegg and Brimblecombe,  
184 1988). The corrected supersaturations were reported in our work.



185

186 **Figure 3.** Activation fractions of methyl-OS and its internally mixed aerosol particles with  
187 ammonium sulfate (AS) as a function of dry particle diameter at four supersaturations.

188

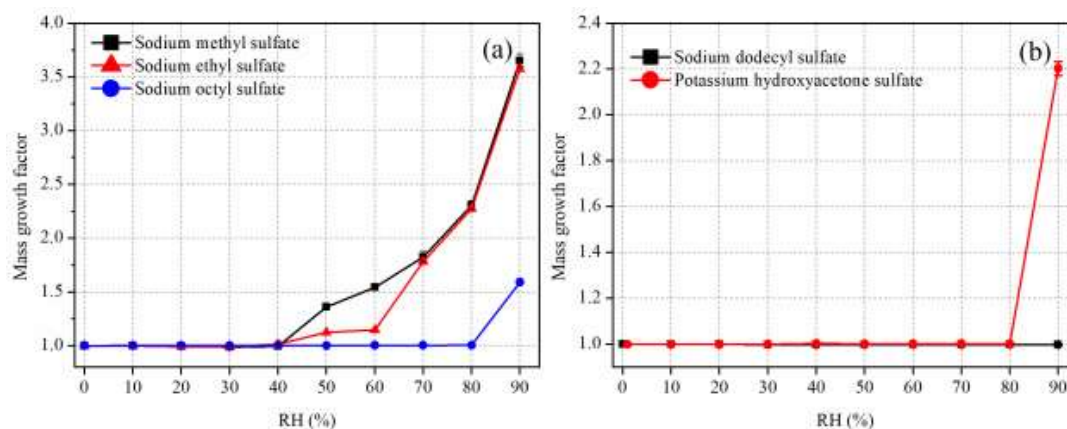
### 189 3 Results and discussion

#### 190 3.1 Mass growth of organosulfates

191 Figure 4 displays mass growth factors of sodium methyl sulfate (methyl-OS), sodium ethyl  
192 sulfate (ethyl-OS), sodium octyl sulfate (octyl-OS), sodium dodecyl sulfate (dodecyl-OS) and



193 potassium hydroxyacetone sulfate, and the data are also listed in Table 1. Figure 4a suggests that  
194 methyl-OS was deliquesced when RH was increased from 40% to 50%, and after that mass growth  
195 factors increased further with RH. The mass of ethyl-OS was moderately increased (by ~11%)  
196 when RH was increased from 40% to 50%, and further increase in RH to 60% led to additional  
197 while small increase in sample mass (by ~2%); the increase in sample mass at 50% and 60% RH  
198 may be because ethyl-OS were partially deliquesced at this stage. When RH was increased to 70%,  
199 ethyl-OS was completely deliquesced, and further increase in RH (to 80% and 90%) resulted in  
200 further increase in sample mass. Octyl-OS was only deliquesced when RH was increased from 80%  
201 to 90%, whereas no significant water uptake was observed for dodecyl-OS even at 90% RH. The  
202 mass growth factors at 90% RH were determined to be  $3.652 \pm 0.064$ ,  $3.575 \pm 0.024$  and  $1.591 \pm 0.004$   
203 for methyl-OS, ethyl-OS and octyl-OS, respectively.



204  
205 **Figure 4.** Mass growth factors of (a) methyl-, ethyl- and octyl-OS and (b) dodecyl-OS and  
206 potassium hydroxyacetone sulfate as a function of RH at 25 °C. Please note that error bars are  
207 included, but they are too small to be clearly visible.

208



209 Mass growth factors of seven potassium organosulfates were also investigated, including  
210 potassium hydroxyacetone sulfate, potassium 3-hydroxy phenyl sulfate, potassium benzyl sulfate,  
211 potassium 2-methyl benzyl sulfate, potassium 3-methyl benzyl sulfate, potassium 2,4-dimethyl  
212 benzyl sulfate and potassium 3,5-dimethyl benzyl sulfate. All the compounds did not show obvious  
213 water uptake at 80% RH. When RH was increased to 90%, as shown in Figure 4b, a significant  
214 increase in mass was observed for potassium hydroxyacetone sulfate particles, suggesting that  
215 occurrence of deliquescence, and the mass growth factor was determined to be  $2.202 \pm 0.031$  at 90%  
216 RH. No significant water uptake was observed for the other six potassium organosulfates even  
217 when RH was increased to 90%. We should mention that occasionally small increase in sample  
218 mass (up to 10-20%) was observed for a few samples when RH was increased from 80% to 90%,  
219 and such small increase in sample mass may be caused by water uptake of impurities (such as  
220 potassium hydroxide) contained in these synthesized compounds.

221

222 **Table 1.** Mass growth factors ( $m/m_0$ ) and water-to-solute ratios (WSRs) as a function of RH (10-  
223 90 %) at 25 °C for sodium methyl sulfate, sodium ethyl sulfate, sodium octyl sulfate and potassium  
224 hydroxyacetone sulfate. All the errors given in this work are standard deviations.

RH (%)	sodium methyl sulfate		sodium ethyl sulfate	
	$m/m_0$	WSR	$m/m_0$	WSR
10	$1.000 \pm 0.003$	-	$1.000 \pm 0.001$	-
20	$1.000 \pm 0.003$	-	$0.992 \pm 0.012$	-
30	$0.989 \pm 0.013$	-	$0.991 \pm 0.012$	-
40	$0.996 \pm 0.018$	-	$1.015 \pm 0.031$	-
50	$1.360 \pm 0.018$	$2.68 \pm 0.04$	$1.125 \pm 0.005$	-
60	$1.545 \pm 0.034$	$4.06 \pm 0.09$	$1.147 \pm 0.004$	-
70	$1.827 \pm 0.051$	$6.16 \pm 0.17$	$1.785 \pm 0.021$	$6.46 \pm 0.07$



80	2.306±0.042	9.73±0.18	2.274±0.024	10.48±0.11
90	3.652±0.064	19.75±0.34	3.575±0.024	21.19±0.14
RH (%)	sodium octyl sulfate		potassium hydroxyacetone sulfate	
	$m/m_0$	WSR	$m/m_0$	WSR
10	1.001±0.001	-	1.000±0.001	-
20	1.002±0.001	-	1.000±0.001	-
30	1.002±0.001	-	1.000±0.001	-
40	1.002±0.001	-	1.003±0.005	-
50	1.003±0.001	-	1.002±0.003	-
60	1.003±0.001	-	1.002±0.004	-
70	1.004±0.001	-	1.003±0.003	-
80	1.005±0.001	-	1.002±0.004	-
90	1.591±0.004	7.63±0.02	2.202±0.031	12.84±0.18

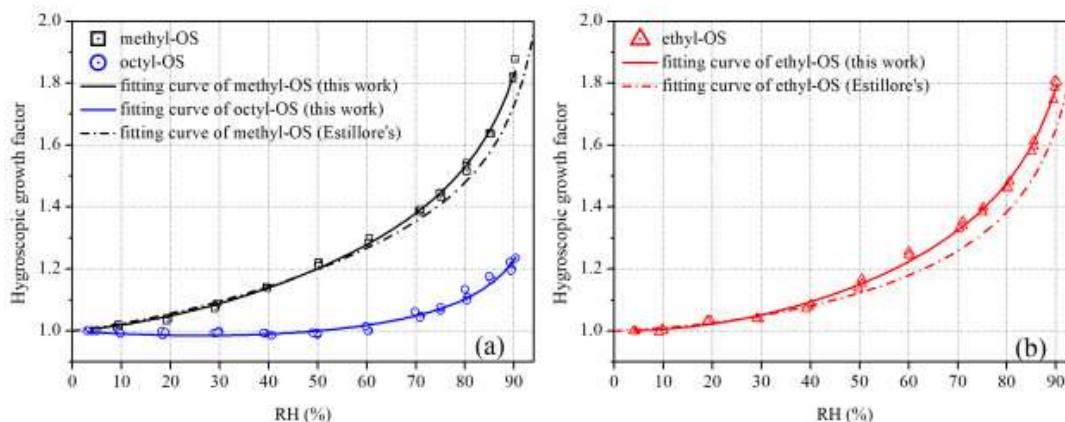
225

226 For deliquesced samples, measured mass changes can be converted to water to solute ratios  
227 (WSRs), defined as the molar ratio of H<sub>2</sub>O to sulfur. The WSRs data are summarized in Table 1  
228 for sodium methyl sulfate, sodium ethyl sulfate, sodium octyl sulfate and potassium  
229 hydroxyacetone sulfate. As shown in Table 1, WSRs at 90% RH were determined to be 19.75±0.34,  
230 21.19±0.14, 7.63±0.02 and 12.84±0.18 for sodium methyl sulfate, sodium ethyl sulfate, sodium  
231 octyl sulfate and potassium hydroxyacetone sulfate at 25 °C.

### 232 3.2 Hygroscopic growth of aerosols

#### 233 3.2.1 Organosulfates

234 H-TDMA was employed to measure hygroscopic growth factors of 100 nm methyl-, ethyl-  
235 and octyl-OS aerosols as a function of RH (up to 90%), and the results are shown in Figure 5 and  
236 Table 2. In addition, no significant hygroscopic growth was observed for dodecyl-OS for RH up  
237 to 90%. We did not investigate hygroscopic growth of other OS aerosols due to the very small  
238 quantity of these synthesized compounds.



239

240 **Figure 5.** Hygroscopic growth factors of (a) methyl- and octyl-OS and (b) ethyl-OS aerosols as a  
241 function of RH. Solid curves represent fitted curves in our work using Eq. (1). For comparison,  
242 the fitted curves reported by Estillore et al. (2016) are presented by dashed curves.

243

244 As shown in Figure 5, methyl-, ethyl- and octyl-OS aerosols all exhibited continuous  
245 hygroscopic growth without obvious phase transitions. To our knowledge, only one previous study  
246 (Estillore et al., 2016) investigated hygroscopic growth of methyl- and ethyl-OS aerosols using a  
247 H-TDMA, and continuous hygroscopic growth was also observed. The continuous growth  
248 behavior can be attributed to the amorphous state of aerosol particles, which would take up water  
249 at very low RH. For methyl-OS aerosol, GFs were determined in our work to be  $1.53 \pm 0.01$ ,  
250  $1.63 \pm 0.01$  and  $1.83 \pm 0.03$  at 80%, 85% and 90% RH; for comparison, its GF was measured to be  
251 1.50 at 85% RH by Estillore et al. (2016), only ~8% smaller than our result. In our work, GFs were  
252 determined to be  $1.47 \pm 0.01$ ,  $1.60 \pm 0.02$  and  $1.79 \pm 0.02$  at 80%, 85% and 90% RH for ethyl-OS  
253 aerosol; for comparison, it was measured to be 1.45 at 85% RH in the previous study (Estillore et  
254 al., 2016), only ~9% smaller than our result. Overall, our measured GFs agree very well with those  
255 reported by Estillore et al. (2016) for methyl- and ethyl-OS, while the highest RH we reached was



256 90%, compared to 85% by Estillore et al. (2016). With respect to octyl-OS aerosol, GF were  
257 determined to be  $1.11 \pm 0.02$ ,  $1.17 \pm 0.01$  and  $1.21 \pm 0.02$  at 80%, 85% and 90% RH in our work; to  
258 our knowledge, hygroscopic growth of octyl-OS aerosol has not been explored previously.  
259 Compared to ammonium sulfate (1.753 at 90% RH), GFs at 90% RHs were found to be slightly  
260 larger for methyl- and ethyl-OS, but significantly smaller for octyl-OS.

261

262 **Table 2.** Hygroscopic growth factors (GFs) of methyl-, ethyl- and octyl-OS aerosols at different  
263 RH. All the errors given in this work are standard deviations.

RH (%)	sodium methyl sulfate	sodium ethyl sulfate	sodium octyl sulfate
5	$1.00 \pm 0.01$	$1.00 \pm 0.01$	$1.00 \pm 0.01$
10	$1.01 \pm 0.01$	$1.00 \pm 0.01$	$1.00 \pm 0.01$
20	$1.04 \pm 0.01$	$1.03 \pm 0.01$	$0.99 \pm 0.01$
30	$1.08 \pm 0.01$	$1.04 \pm 0.01$	$1.00 \pm 0.01$
40	$1.14 \pm 0.01$	$1.08 \pm 0.01$	$0.99 \pm 0.01$
50	$1.22 \pm 0.01$	$1.15 \pm 0.01$	$0.99 \pm 0.01$
60	$1.29 \pm 0.01$	$1.25 \pm 0.01$	$1.01 \pm 0.01$
70	$1.39 \pm 0.01$	$1.34 \pm 0.01$	$1.05 \pm 0.01$
75	$1.44 \pm 0.01$	$1.39 \pm 0.01$	$1.07 \pm 0.01$
80	$1.53 \pm 0.01$	$1.47 \pm 0.01$	$1.11 \pm 0.02$
85	$1.63 \pm 0.01$	$1.60 \pm 0.02$	$1.17 \pm 0.01$
90	$1.83 \pm 0.03$	$1.79 \pm 0.02$	$1.21 \pm 0.02$

264

265 When aerosol particles take up water continuously, the RH-dependent GFs can usually be  
266 fitted using Eq. (1) (Kreidenweis et al., 2005):

267

$$\text{GF} = \left[ 1 + \left( a + b \cdot \frac{\text{RH}}{100} + c \cdot \left( \frac{\text{RH}}{100} \right)^2 \right) \cdot \frac{\text{RH}}{100 - \text{RH}} \right]^{1/3} \quad (1)$$





268 where  $a$ ,  $b$  and  $c$  are coefficients obtained from fitting using Eq. (1). As shown in Figure 5,  
269 hygroscopic growth factors of methyl-, ethyl- and octyl-OS aerosols can be fitted by Eq. (1), and  
270 the obtained coefficients ( $a$ ,  $b$  and  $c$ ) are summarized in Table 3.

271

272 **Table 3.** The three coefficients ( $a$ ,  $b$  and  $c$ ) obtained by using Eq. (1) to fit RH-dependent GFs for  
273 sodium methyl sulfate, sodium ethyl sulfate and sodium octyl sulfate aerosols.

organosulfates	$a$	$b$	$c$
sodium methyl sulfate	0.42182	1.20336	-1.15508
sodium ethyl sulfate	0.00174	1.61805	-1.15502
sodium octyl sulfate	-0.31868	0.86233	-0.44623

274

### 275 3.2.2 Comparison between VSA and H-TDMA measurements

276 Figure 4 shows that obvious deliquescence transitions were observed for methyl-, ethyl-, and  
277 octyl-OS in the VSA experiments; in contrast, as revealed by Figure 5, continuous hygroscopic  
278 growth without obvious phase transitions was observed for methyl-, ethyl- and octyl-OS aerosol  
279 particles in H-TDMA measurements, suggesting that these aerosol particles may exist in  
280 amorphous state. Estillore et al. (2016) employed a H-TDMA to investigate hygroscopic properties  
281 of several OS aerosols, and similarly they found that those aerosols, including methyl-OS, ethyl-  
282 OS and potassium hydroxyacetone sulfate which were also examined in our work, displayed  
283 continuous hygroscopic growth.

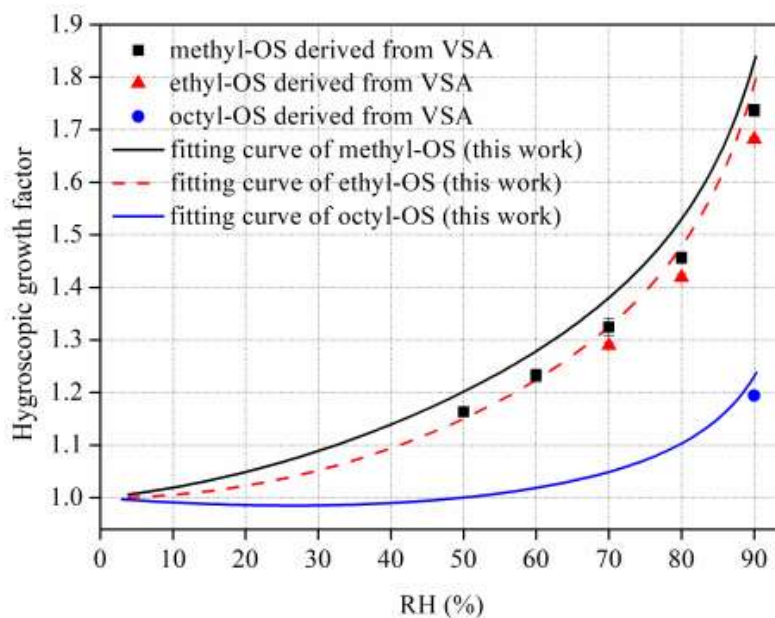
284 For completely deliquesced particles, if it is assumed that the particle is spherical and that the  
285 particle volume at a given RH is equal to the sum of the dry particle volume and the volume of



286 particulate water, particle mass change, measured using the VSA, can then be converted to  
287 hygroscopic GF, using Eq. (2):

$$288 \quad GF = \sqrt[3]{1 + \left(\frac{m}{m_0} - 1\right) \cdot \frac{\rho_0}{\rho_w}} \quad (2)$$

289 where  $\rho_0$  and  $\rho_w$  are the density of the dry sample and water, respectively. The density of methyl-,  
290 ethyl- and octyl-OS particles were reported to be 1.60, 1.46 and 1.19 g cm<sup>-3</sup> with an uncertainty of  
291 20-30% (Kwong et al., 2018; ChemistryDashboard, 2021). Figure 6 compares VSA-derived GFs  
292 and those measured using H-TDMA for methyl-, ethyl- and octyl-OS, and it can be concluded that  
293 for RH at which samples used in the VSA experiments were deliquesced, GFs derived from mass  
294 change measured using VSA agree relatively well with those directly measured using H-TDMA.  
295 For example, at 90% RH GFs were measured by H-TDMA to be 1.83±0.03, 1.79±0.02 and  
296 1.21±0.02 for methyl-, ethyl- and octyl-OS, while at the same RH their GFs derived from VSA  
297 measurements were found to be 1.74±0.01, 1.68±0.01 and 1.19±0.01, only 6% (or less) smaller  
298 than those measured using H-TDMA.



299



300 **Figure 6.** Comparison between hygroscopic GFs of methyl-, ethyl- and octyl-OS derived from  
301 VSA experiments to those measured using H-TDMA. Please note that H-TDMA results are  
302 presented as the three-parameter curves obtained. Error bars are included, but they are too small  
303 to be clearly visible.

304

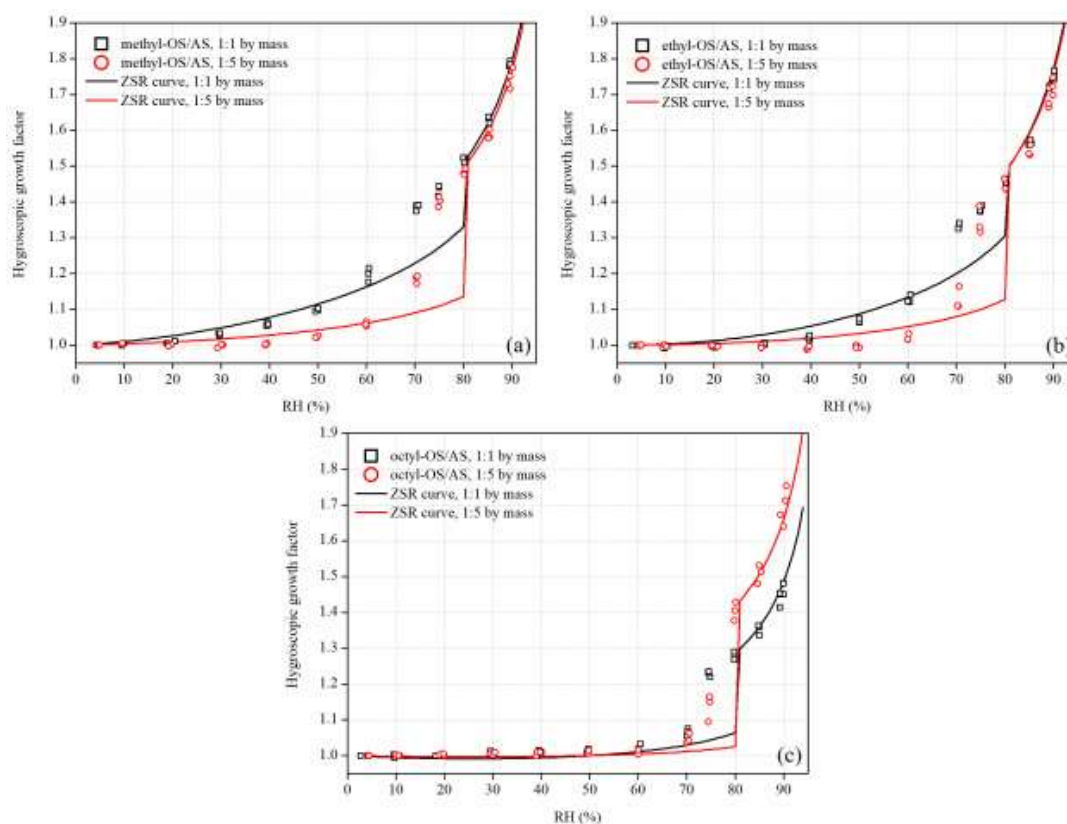
### 305 **3.2.3 Internally mixed aerosols**

306 We also investigated hygroscopic properties of methyl-, ethyl- and octyl-OS aerosols  
307 internally mixed with ammonium sulfate (AS), and the results are summarized in Table 4. Figure  
308 7a displays GFs of 100 nm methyl-OS/AS mixed aerosols with mass ratios of 1:1 and 1:5. The 1:1  
309 mixed aerosol particle showed a deliquescence transition at 70% RH, while the 1:5 mixed aerosols  
310 showed a deliquescence transition at 75% RH, which was lower than the deliquescence RH (DRH,  
311 80%) of AS. Here the DRH is defined as the RH at which the mixed aerosols are completely  
312 deliquesced (Choi and Chan, 2002). Figure 7a suggests that before full deliquescence, significant  
313 hygroscopic growth was also observed, i.e. pre-deliqescence of mixed particles occurred when  
314 RH was lower than their DRH. Pre-deliqescence was widely reported in previous studies which  
315 investigated hygroscopic properties of inorganic/organic mixed aerosols (Choi and Chan, 2002;  
316 Prenni, 2003; Wise et al., 2003; Brooks, 2004; Marcolli and Krieger, 2006; Wu et al., 2011; Lei et  
317 al., 2014; Jing et al., 2016; Estillore et al., 2017). For example, Choi and Chan. (2002) investigated  
318 hygroscopic behaviors of internal mixed particles which consisted of water-soluble organic  
319 compounds and AS, and found that the internal mixing with organics (such as malonic and citric  
320 acids) could reduce the DRH of AS, due to the ability of organics to absorb water at low RH.

321 Internal mixing with ethyl- and octyl-OS could also reduce the DRH of AS. As shown in  
322 Figure 7b, ethyl-OS/AS mixed aerosols were deliquesced at 70% RH when the mass ratio of ethyl-



323 OS to AS was 1:1 and at 80% RH when the mass ratio was 1:5. In addition, Figure 7c suggested  
324 that the deliquescence of octyl-OS/AS aerosols took place at 75% RH for the 1:1 mixture and at  
325 80% for 1:5 mixture.



326  
327 **Figure 7.** Hygroscopic growth factors of (a) methyl-OS/AS, (b) ethyl-OS/AS, and (c) octyl-OS/AS  
328 aerosols as a function of RH. The mass ratios of methyl-, ethyl-, and octyl-OS to AS were 1:1 and  
329 1:5, respectively. Solid curves represent hygroscopic growth factors of mixed aerosols predicted  
330 using the ZSR method.

331

332 **Table 4.** Hygroscopic GF of methyl-, ethyl-, and octyl-OS internally mixed with AS (their mass  
333 ratios are 1:1 and 1:5) at different RH. All the errors given in this work are standard deviations.



RH (%)	methyl-OS/AS		ethyl-OS/AS		octyl-OS/AS	
	1:1	1:5	1:1	1:5	1:1	1:5
5	1.00±0.01	1.00±0.01	1.00±0.01	1.00±0.01	1.00±0.01	1.00±0.01
10	1.00±0.01	1.00±0.01	1.00±0.01	1.00±0.01	1.00±0.01	1.00±0.01
20	1.01±0.01	1.00±0.01	1.00±0.01	1.00±0.01	1.00±0.01	1.00±0.01
30	1.03±0.01	1.00±0.01	1.00±0.01	1.00±0.01	1.01±0.01	1.01±0.01
40	1.06±0.01	1.00±0.01	1.02±0.01	0.99±0.01	1.01±0.01	1.01±0.01
50	1.10±0.01	1.02±0.01	1.07±0.01	0.99±0.01	1.01±0.01	1.01±0.01
60	1.20±0.02	1.06±0.01	1.13±0.01	1.02±0.01	1.02±0.01	1.01±0.01
70	1.38±0.01	1.19±0.01	1.33±0.01	1.13±0.03	1.07±0.01	1.05±0.01
75	1.43±0.01	1.40±0.01	1.38±0.01	1.34±0.04	1.23±0.01	1.14±0.03
80	1.52±0.01	1.48±0.01	1.46±0.01	1.45±0.02	1.28±0.01	1.40±0.02
85	1.63±0.01	1.59±0.01	1.56±0.01	1.54±0.02	1.35±0.02	1.51±0.02
90	1.79±0.01	1.74±0.02	1.74±0.02	1.72±0.02	1.47±0.02	1.69±0.04

334

335 The Zdanovskii-Stokes-Robinson (ZSR) method (Stokes and Robinson, 1966) has been  
336 widely used to predict hygroscopic growth of internally mixed aerosol particles, assuming that the  
337 interaction among individual species are negligible and that individual species in the mixed  
338 particles take up water independently. According to the ZSR method, GF of a mixed particle,  $GF_{\text{mix}}$ ,  
339 can be calculated using Eq. (3) (Malm and Kreidenweis, 1997):

340 
$$GF_{\text{mix}} = \sqrt[3]{\sum(\varepsilon_i \cdot GF_i^3)} \quad (3)$$

341 where  $GF_i$  is the GF of  $i$ th species the dry mixed particle contains. The volume fraction of the  $i$ th  
342 species in the dry mixed particle,  $\varepsilon_i$ , can be calculated using Eq. (4):

343 
$$\varepsilon_i = \frac{m_i/\rho_i}{\sum(m_i/\rho_i)} \quad (4)$$

344 where  $m_i$  and  $\rho_i$  are the mass fraction and density of the  $i$ th species. GFs of pure OS, measured in  
345 our work using H-TDMA and presented in Section 3.2.1, and GFs of AS, calculated using the E-



346 AIM model (Clegg et al., 1998; Wexler and Clegg, 2002), were used as input to predict GFs of  
347 methyl-, ethyl- and octyl-OS internally mixed with AS. Comparisons between measured and  
348 predicted GFs are displayed in Figure 7 for OS/AS mixed aerosols.

349 As shown in Figure 7a, GFs of methyl-OS/AS mixed aerosols (both the 1:1 and 1:5 mixtures)  
350 could be well predicted using the ZSR method when RH was <60% or >80%, while the ZSR  
351 method underestimated their GFs at 70% and 75% RH. Such underestimation at 70% and 75% RH  
352 is likely to due to that inorganic compounds (AS, in our work) may dissolve partially in the  
353 organics/water solution (which can be formed at much lower RH due to continuous water uptake  
354 of organics) before the mixed particle is completely deliquesced (Svenningsson et al., 2006;  
355 Zardini et al., 2008; Wu et al., 2011); in contrast, the ZSR method assumes that individual species  
356 take up water independently. As shown in Figure 7, the ZSR method also underestimated GFs at  
357 70 and 75% RH for ethyl-OS/AS and octyl-OS/AS mixed aerosols, though good agreement  
358 between measurement and prediction was found at other RH.

### 359 **3.3 Cloud condensation nucleation activities**

360 Figures 3, S2 and S3 show CCN activation curves obtained at four supersaturations for  
361 methyl-, ethyl- and octyl-OS aerosols and their internal mixtures with ammonium sulfate. Each  
362 activation curve was fitted using a Boltzmann sigmoid function to derive the corresponding critical  
363 particle diameter ( $d_{50}$ ), which was then used to calculate  $\kappa_{\text{ccn}}$  using Eqs. (5a-5b) (Petters and  
364 Kreidenweis, 2007):

$$365 \quad \kappa_{\text{ccn}} = \frac{4A^3}{27d_{50}^3 \ln^2 S_c} \quad (5a)$$

$$366 \quad A = \frac{4\sigma_s/a M_w}{RT\rho_w} \quad (5b)$$

367 where  $S_c$  is the critical saturation ratio ( $1+SS$ ) of water;  $d_{50}$  is the critical particle diameter;  $A$  is a  
368 constant which describes the Kelvin effect on a curved surface of a droplet, and depends on the



369 surface tension ( $\sigma_{s/a}$ ), molecular weight ( $M_w$ ), density ( $\rho_w$ ) of water, temperature ( $T$ ) and the  
 370 universal gas constant ( $R$ ). Table 5 summarizes critical diameters at different supersaturations for  
 371 aerosol particles examined in this work and their  $\kappa_{ccn}$  values.

372

373 **Table 5.** Single hygroscopicity parameters derived from hygroscopic growth ( $\kappa_{gf}$ ) and CCN  
 374 activity measurements ( $\kappa_{ccn}$ ) for methyl-, ethyl- and octyl-OS and their internal mixtures with  
 375 ammonium sulfate (AS). All errors given were standard deviations.

aerosol	mass ratio	SS (%)	$d_{50}$ (nm)	$\kappa_{ccn}$	average $\kappa_{ccn}$	$\kappa_{gf}$
methyl-OS	-	0.45	52.9±0.9	0.432-0.477	0.459±0.021	0.537-0.604
	-	0.67	41.1±0.8	0.416-0.468		
	-	0.87	33.3±0.4	0.471-0.507		
	-	1.13	28.8±0.5	0.431-0.477		
methyl-OS/AS	1:5	0.45	51.9±0.5	0.467-0.492	0.453±0.027	0.454-0.495
	1:5	0.67	41.6±0.4	0.411-0.436		
	1:5	0.87	33.7±0.5	0.453-0.490		
	1:5	1.13	29.2±0.6	0.412-0.464		
ethyl-OS	-	0.45	55.5±0.8	0.375-0.410	0.397±0.010	0.505-0.548
	-	0.67	42.8±0.6	0.376-0.406		
	-	0.87	35.3±0.5	0.395-0.428		
	-	1.13	30.2±0.3	0.382-0.408		
ethyl-OS/AS	1:5	0.45	52.3±1.2	0.437-0.504	0.458±0.024	0.435-0.474
	1:5	0.67	41.0±0.5	0.426-0.459		
	1:5	0.87	33.4±0.6	0.463-0.512		
	1:5	1.13	29.2±0.6	0.409-0.462		
octyl-OS	-	0.45	70.0±1.2	0.186-0.207	0.206±0.008	0.076-0.096
	-	0.67	53.2±0.6	0.196-0.211		
	-	0.87	44.1±0.7	0.202-0.221		
	-	1.13	37.1±0.8	0.200-0.227		
octyl-OS/AS	1:5	0.45	53.7±0.9	0.413-0.456	0.436±0.009	0.388-0.464



1:5	0.67	41.1±0.5	0.426-0.458
1:5	0.87	34.4±0.5	0.427-0.462
1:5	1.13	29.5±0.2	0.413-0.434

376

377 As shown in Table 5,  $\kappa_{\text{ccn}}$  values were determined to be  $0.459 \pm 0.021$ ,  $0.397 \pm 0.010$  and  
378  $0.206 \pm 0.008$  for methyl-, ethyl- and octyl-OS, decreasing with alkyl chain length, and this suggests  
379 that the addition of hydrophobic hydrocarbon functional groups to OS reduced their hygroscopicity.  
380 In addition, we investigated CCN activities of alkyl-OS/AS mixed aerosols with a mass ratio of  
381 1:5, and  $\kappa_{\text{ccn}}$  values were determined to be  $0.453 \pm 0.027$ ,  $0.458 \pm 0.024$  and  $0.436 \pm 0.009$  for methyl-  
382 OS/AS, ethyl-OS/AS and octyl-OS/AS.

### 383 3.3.1 Comparison between H-TDMA and CCN activities measurements

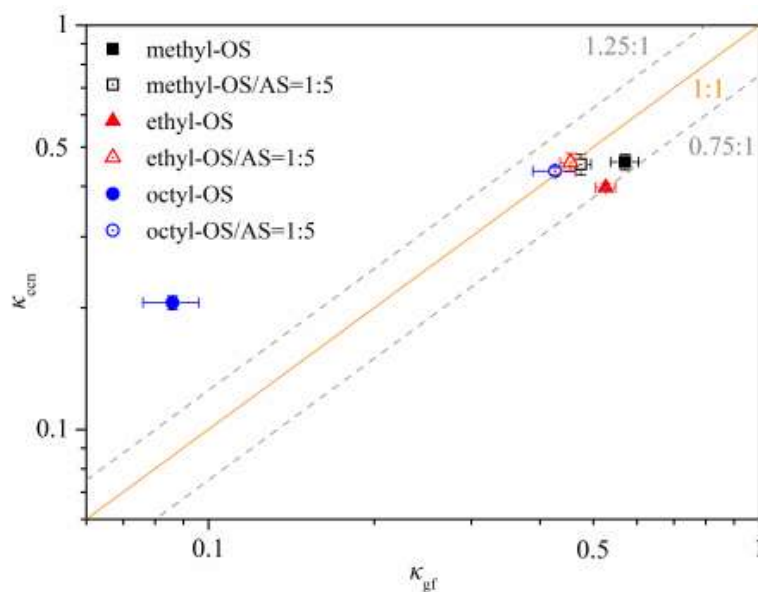
384 It is suggested that the single hygroscopicity parameter,  $\kappa$ , could describe aerosol-water  
385 interactions under both sub- and supersaturated conditions (Petters and Kreidenweis, 2007). The  $\kappa$   
386 values derived from CCN activity measurements,  $\kappa_{\text{ccn}}$ , have been illustrated above; the  $\kappa$  values  
387 derived from H-TDMA measurements,  $\kappa_{\text{gf}}$ , can be calculated using Eq. (6) (Petters and  
388 Kreidenweis, 2007; Tang et al., 2016):

$$389 \kappa_{\text{gf}} = (\text{GF}^3 - 1) \frac{1 - \text{RH}}{\text{RH}} \quad (6)$$

390 In this work GF measured at 90% RH were used to calculate  $\kappa_{\text{gf}}$  values, which are also listed in  
391 Table 5.

392 Figure 8 compares  $\kappa_{\text{ccn}}$  and  $\kappa_{\text{gf}}$  values for the six types of aerosol particles examined. No  
393 significant difference was observed between  $\kappa_{\text{gf}}$  and  $\kappa_{\text{ccn}}$  for five types of aerosol particles, and the  
394 relative differences between  $\kappa_{\text{ccn}}$  and  $\kappa_{\text{gf}}$  values do not exceed 25%. However, octyl-OS appears to  
395 be an exception, and the average  $\kappa_{\text{ccn}}$  value (0.206) was ~1.4 times larger than the average  $\kappa_{\text{gf}}$  value  
396 (0.086).





397

398 **Figure 8.** Comparison of  $\kappa$  values derived from hygroscopic growth ( $\kappa_{gf}$ ) with these derived from  
399 CCN activities ( $\kappa_{ccn}$ ) for methyl-, ethyl- and octyl-OS aerosols as well as their internal mixtures  
400 with ammonium sulfate (the mass ratio was 1:5).

401

402 Significant differences between  $\kappa_{gf}$  and  $\kappa_{ccn}$  were reported in previous studies (Petters et al.,  
403 2009; Wex et al., 2009; Hansen et al., 2015), attributed to several factors discussed below. Petters  
404 and Kreidenweis. (2008) demonstrated that cloud droplet activation was highly sensitive to the  
405 solubility for sparingly soluble compounds in the range of  $5 \times 10^{-4}$ - $2 \times 10^{-1}$ , expressed as volume of  
406 solute per unit volume of water (Petters and Kreidenweis, 2008). Compared to the highly soluble  
407 methyl- and ethyl-OS, the solubility of octyl-OS ( $8.43 \times 10^{-4}$ - $4.26 \times 10^{-2}$ ) (Chemistry Dashboard,  
408 2021) is rather limited, and incomplete dissolution at subsaturated condition in H-TDMA  
409 measurements may lead to underestimation of  $\kappa_{gf}$  values for octyl-OS; as a result, the solubility  
410 limit may explain the observed difference between  $\kappa_{gf}$  and  $\kappa_{ccn}$  for octyl-OS. Furthermore, surface



411 tension is a key factor to influence critical supersaturations at which aerosol particles are activated  
412 to cloud droplets (Petters and Kreidenweis, 2013). We measured surface tensions of alkyl-OS and  
413 alkyl-OS/AS (the mass ratio was 1:5) solutions, and the results are shown in Table S1 and Figure  
414 S4. The surface tension of octyl-OS is much lower than that of pure water, leading to significant  
415 reduction in critical supersaturations and thus overestimation of its  $\kappa_{\text{ccn}}$  value; for comparison, the  
416 surface tension depression is also visible but much less pronounced for octyl-OS/AS. Overall, we  
417 proposed that solubility limit and surface tension reduction may both contribute to the observed  
418 discrepancy between  $\kappa_{\text{gf}}$  and  $\kappa_{\text{ccn}}$  values for octyl-OS aerosol.

#### 419 **4. Conclusions**

420 Organosulfates (OS) may contribute significantly to secondary organic aerosols in various  
421 locations over the globe; however, their hygroscopic properties and CCN activities have not been  
422 well understood. In this work, three complementary techniques, including a vapor sorption  
423 analyzer (VSA), a hygroscopicity tandem differential mobility analyzer (H-TDMA) and a cloud  
424 condensation nuclei counter (CCNc), were employed to investigate interactions of several OS with  
425 water vapor under sub- and supersaturated conditions, trying to get a comprehensive picture of  
426 their hygroscopic properties and CCN activities.

427 VSA was used to measure mass change of OS samples with RH (0-90%). Obvious  
428 deliquescence was found for sodium methyl sulfate (methyl-OS), sodium ethyl sulfate (ethyl-OS),  
429 sodium octyl sulfate (octyl-OS) and potassium hydroxyacetone sulfate, and their mass growth  
430 factors at 90% RH were determined to be  $3.652 \pm 0.064$ ,  $3.575 \pm 0.024$ ,  $1.591 \pm 0.004$  and  
431  $2.202 \pm 0.031$ , respectively. No significant water uptake were observed up to 90% RH for other OS  
432 compounds examined, including sodium dodecyl sulfate, potassium 3-hydroxy phenyl sulfate,  
433 potassium benzyl sulfate, potassium 2-methyl benzyl sulfate, potassium 3-methyl benzyl sulfate,



434 potassium 2,4-dimethyl benzyl sulfate and potassium 3,5-dimethyl benzyl sulfate. Hygroscopic  
435 properties of methyl-, ethyl- and octyl-OS aerosols were also studied using H-TDMA, which  
436 measured mobility diameters of aerosol particles as a function of RH. Continuous hygroscopic  
437 growth was observed for methyl-, ethyl- and octyl-OS aerosols, and their growth factors at 90%  
438 RH were measured to be  $1.83 \pm 0.03$ ,  $1.79 \pm 0.02$  and  $1.21 \pm 0.02$ .

439 We further investigated CCN activities of methyl-, ethyl- and octyl-OS aerosols, and their  
440 single hygroscopicity parameters,  $\kappa_{\text{ccn}}$ , were determined to be  $0.459 \pm 0.021$ ,  $0.397 \pm 0.010$  and  
441  $0.206 \pm 0.008$ , respectively. For methyl- and ethyl-OS aerosols, single hygroscopicity parameters  
442 derived from CCN activities ( $\kappa_{\text{ccn}}$ ) agree reasonably well with those derived from H-TDMA  
443 measurements ( $\kappa_{\text{gf}}$ ). However,  $\kappa_{\text{ccn}}$  was found to be significantly larger than  $\kappa_{\text{gf}}$  for octyl-OS, and  
444 we show that solubility limit and surface tension reduction may both contribute to such  
445 discrepancy observed.

446

447 **Data availability.** Data used in this paper can be found in the main text or supplement.

448 **Competing interests.** The authors declare that they have no conflict of interest.

449 **Author contribution.** Mingjin Tang conceived this work; Ru-Jin Huang, Yuqing Zhang, Xiang  
450 Ding and Xinming Wang chose and provided samples investigated in this work; Chao Peng,  
451 Lanxiadi Chen, Yuqing Zhang and Xiang Ding conducted VSA measurements; Chao Peng,  
452 Weigang Wang and Maofa Ge conducted H-TDMA measurements; Patricia N. Razafindrambinina,  
453 Kotiba A. Malek and Akua A. Asa-Awuku conducted CCN activity measurements; Chao Peng,  
454 Patricia N. Razafindrambinina, Kotiba A. Malek, Akua A. Asa-Awuku and Mingjin Tang analyzed  
455 the data and prepared the manuscript with contribution from all the other coauthors.



## 456 Financial support

457 This work was funded by National Natural Science Foundation of China (91744204), China  
458 Postdoctoral Science Foundation (2020M682931), State Key Laboratory of Loess and Quaternary  
459 Geology (SKLLQG1921), Guangdong Foundation for Program of Science and Technology  
460 Research (2017B030314057, 2019B121205006 and 2020B1212060053), Guangdong Science and  
461 Technology Department (2017GC010501) and CAS Pioneer Hundred Talents program.

462

## 463 References

- 464 Brooks, S.: Water uptake by particles containing humic materials and mixtures of humic materials with ammonium  
465 sulfate, *Atmos. Environ.*, 38, 1859-1868, 2004.
- 466 Brüggemann, M., Xu, R., Tilgner, A., Kwong, K. C., Mutzel, A., Poon, H. Y., Otto, T., Schaefer, T., Poulain, L., Chan,  
467 M. N., and Herrmann, H.: Organosulfates in Ambient Aerosol: State of Knowledge and Future Research  
468 Directions on Formation, Abundance, Fate, and Importance, *Environmental science & technology*, 2020.
- 469 ChemistryDashboard: United States Environmental Protection Agency, available at:  
470 <https://comptox.epa.gov/dashboard>, last access: 12 January 2021, in, 2021.
- 471 Chen, L., Chen, Y., Chen, L., Gu, W., Peng, C., Luo, S., Song, W., Wang, Z., and Tang, M.: Hygroscopic Properties  
472 of 11 Pollen Species in China, *ACS Earth and Space Chemistry*, 3, 2678-2683, 2019.
- 473 Choi, M. Y., and Chan, C. K.: The effects of organic species on the hygroscopic behaviors of inorganic aerosols,  
474 *Environ. Sci. Technol.*, 36, 2422-2428, 2002.
- 475 Clegg, S. L., and Brimblecombe, P.: Equilibrium partial pressures of strong acids over concentrated saline solutions-  
476 I. HNO<sub>3</sub>, *Atmospheric Environment*, 22, 91-100, 1988.
- 477 Clegg, S. L., Brimblecombe, P., and Wexler, A. S.: Thermodynamic model of the system H<sup>+</sup>-NH<sub>4</sub><sup>+</sup>-Na<sup>+</sup>-SO<sub>4</sub><sup>2-</sup>-  
478 NB<sub>3</sub>-Cl<sup>-</sup>-H<sub>2</sub>O at 298.15 K, *J. Phys. Chem. A*, 102, 2155-2171, 1998.
- 479 Ervens, B., Turpin, B., and Weber, R.: Secondary organic aerosol formation in cloud droplets and aqueous particles  
480 (aqSOA): a review of laboratory, field and model studies, *Atmospheric Chemistry and Physics*, 11, 11069-11102,  
481 2011.
- 482 Estillore, A. D., Hettiyadura, A. P. S., Qin, Z., Leckrone, E., Wombacher, B., Humphry, T., Stone, E. A., and Grassian,  
483 V. H.: Water Uptake and Hygroscopic Growth of Organosulfate Aerosol, *Environmental Science & Technology*,  
484 50, 4259-4268, 2016.
- 485 Estillore, A. D., Morris, H. S., Or, V. W., Lee, H. D., Alves, M. R., Marciano, M. A., Laskina, O., Qin, Z., Tivanski,  
486 A. V., and Grassian, V. H.: Linking hygroscopicity and the surface microstructure of model inorganic salts,  
487 simple and complex carbohydrates, and authentic sea spray aerosol particles, *Physical Chemistry Chemical  
488 Physics*, 19, 21101-21111, 2017.
- 489 Froyd, K. D., Murphy, S. M., Murphy, D. M., de Gouw, J. A., Eddingsaas, N. C., and Wennberg, P. O.: Contribution  
490 of isoprene-derived organosulfates to free tropospheric aerosol mass, *Proceedings of the National Academy of  
491 Sciences of the United States of America*, 107, 21360-21365, 2010.
- 492 Gu, W., Li, Y., Zhu, J., Jia, X., Lin, Q., Zhang, G., Ding, X., Song, W., Bi, X., Wang, X., and Tang, M.: Investigation  
493 of water adsorption and hygroscopicity of atmospherically relevant particles using a commercial vapor sorption  
494 analyzer, *Atmospheric Measurement Techniques*, 10, 3821-3832, 2017.
- 495 Guo, L., Gu, W., Peng, C., Wang, W., Li, Y. J., Zong, T., Tang, Y., Wu, Z., Lin, Q., Ge, M., Zhang, G., Hu, M., Bi,  
496 X., Wang, X., and Tang, M.: A comprehensive study of hygroscopic properties of calcium- and magnesium-  
497 containing salts: implication for hygroscopicity of mineral dust and sea salt aerosols, *Atmospheric Chemistry  
498 and Physics*, 19, 2115-2133, 2019.



- 499 Hallquist, M., Wenger, J. C., Baltensperger, U., Rudich, Y., Simpson, D., Claeys, M., Dommen, J., Donahue, N. M.,  
500 George, C., Goldstein, A. H., Hamilton, J. F., Herrmann, H., Hoffmann, T., Iinuma, Y., Jang, M., Jenkin, M. E.,  
501 Jimenez, J. L., Kiendler-Scharr, A., Maenhaut, W., McFiggans, G., Mentel, T. F., Monod, A., Prevot, A. S. H.,  
502 Seinfeld, J. H., Surratt, J. D., Szmigielski, R., and Wildt, J.: The formation, properties and impact of secondary  
503 organic aerosol: current and emerging issues, *Atmospheric Chemistry And Physics*, 9, 5155-5236, 2009.
- 504 Hansen, A. M. K., Kristensen, K., Nguyen, Q. T., Zare, A., Cozzi, F., Nojgaard, J. K., Skov, H., Brandt, J., Christensen,  
505 J. H., Strom, J., Tunved, P., Krejci, R., and Glasius, M.: Organosulfates and organic acids in Arctic aerosols:  
506 speciation, annual variation and concentration levels, *Atmospheric Chemistry and Physics*, 14, 7807-7823, 2014.
- 507 Hansen, A. M. K., Hong, J., Raatikainen, T., Kristensen, K., Ylisirmio, A., Virtanen, A., Petaja, T., Glasius, M., and  
508 Prisle, N. L.: Hygroscopic properties and cloud condensation nuclei activation of limonene-derived  
509 organosulfates and their mixtures with ammonium sulfate, *Atmospheric Chemistry and Physics*, 15, 14071-14089,  
510 2015.
- 511 He, Q.-F., Ding, X., Wang, X.-M., Yu, J.-Z., Fu, X.-X., Liu, T.-Y., Zhang, Z., Xue, J., Chen, D.-H., Zhong, L.-J., and  
512 Donahue, N. M.: Organosulfates from Pinene and Isoprene over the Pearl River Delta, South China: Seasonal  
513 Variation and Implication in Formation Mechanisms, *Environmental Science & Technology*, 48, 9236-9245,  
514 2014.
- 515 Heald, C. L., Jacob, D. J., Park, R. J., Russell, L. M., Huebert, B. J., Seinfeld, J. H., Liao, H., and Weber, R. J.: A  
516 large organic aerosol source in the free troposphere missing from current models, *Geophysical Research Letters*,  
517 32, 2005.
- 518 Hettiyadura, A. P. S., Stone, E. A., Kundu, S., Baker, Z., Geddes, E., Richards, K., and Humphry, T.: Determination  
519 of atmospheric organosulfates using HILIC chromatography with MS detection, *Atmospheric Measurement*  
520 *Techniques*, 8, 2347-2358, 2015.
- 521 Hettiyadura, A. P. S., Jayarathne, T., Baumann, K., Goldstein, A. H., de Gouw, J. A., Koss, A., Keutsch, F. N., Skog,  
522 K., and Stone, E. A.: Qualitative and quantitative analysis of atmospheric organosulfates in Centreville, Alabama,  
523 *Atmospheric Chemistry and Physics*, 17, 1343-1359, 2017.
- 524 Huang, R.-J., Cao, J., Chen, Y., Yang, L., Shen, J., You, Q., Wang, K., Lin, C., Xu, W., Gao, B., Li, Y., Chen, Q.,  
525 Hoffmann, T., O'Dowd, C. D., Bilde, M., and Glasius, M.: Organosulfates in atmospheric aerosol: synthesis and  
526 quantitative analysis of PM<sub>2.5</sub> from Xi'an, northwestern China, *Atmospheric Measurement Techniques*, 11,  
527 3447-3456, 2018.
- 528 Hughes, D. D., and Stone, E. A.: Organosulfates in the Midwestern United States: abundance, composition and  
529 stability, *Environmental Chemistry*, 16, 312-322, 2019.
- 530 Jimenez, J., Canagaratna, M., Donahue, N., Prevot, A., Zhang, Q., Kroll, J. H., DeCarlo, P. F., Allan, J. D., Coe, H.,  
531 and Ng, N.: Evolution of organic aerosols in the atmosphere, *Science*, 326, 1525-1529, 2009.
- 532 Jing, B., Tong, S., Liu, Q., Li, K., Wang, W., Zhang, Y., and Ge, M.: Hygroscopic behavior of multicomponent organic  
533 aerosols and their internal mixtures with ammonium sulfate, *Atmospheric Chemistry and Physics*, 16, 4101-4118,  
534 2016.
- 535 Kanakidou, M., Seinfeld, J., Pandis, S., Barnes, I., Dentener, F., Facchini, M., Dingenen, R. V., Ervens, B., Nenes, A.,  
536 and Nielsen, C.: Organic aerosol and global climate modelling: a review, *Atmospheric Chemistry and Physics*,  
537 5, 1053-1123, 2005.
- 538 Kreidenweis, S. M., Koehler, K., DeMott, P. J., Prenni, A. J., Carrico, C., and Ervens, B.: Water activity and activation  
539 diameters from hygroscopicity data - Part I: Theory and application to inorganic salts, *Atmospheric Chemistry*  
540 *and Physics*, 5, 1357-1370, 2005.
- 541 Kristensen, K., and Glasius, M.: Organosulfates and oxidation products from biogenic hydrocarbons in fine aerosols  
542 from a forest in North West Europe during spring, *Atmospheric Environment*, 45, 4546-4556, 2011.
- 543 Kundu, S., Quraishi, T. A., Yu, G., Suarez, C., Keutsch, F. N., and Stone, E. A.: Evidence and quantitation of aromatic  
544 organosulfates in ambient aerosols in Lahore, Pakistan, *Atmospheric Chemistry and Physics*, 13, 4865-4875,  
545 2013.
- 546 Kwong, K. C., Chim, M. M., Davies, J. F., Wilson, K. R., and Chan, M. N.: Importance of sulfate radical anion  
547 formation and chemistry in heterogeneous OH oxidation of sodium methyl sulfate, the smallest organosulfate,  
548 *Atmospheric Chemistry and Physics*, 18, 2809-2820, 2018.
- 549 Lance, S., Medina, J., Smith, J. N., and Nenes, A.: Mapping the operation of the DMT Continuous Flow CCN counter,  
550 *Aerosol Science and Technology*, 40, 242-254, 2006.
- 551 Lei, T., Zuend, A., Wang, W. G., Zhang, Y. H., and Ge, M. F.: Hygroscopicity of organic compounds from biomass  
552 burning and their influence on the water uptake of mixed organic ammonium sulfate aerosols, *Atmos. Chem.*  
553 *Phys.*, 14, 11165-11183, 2014.



- 554 Liao, J., Froyd, K. D., Murphy, D. M., Keutsch, F. N., Yu, G., Wennberg, P. O., St. Clair, J. M., Crouse, J. D.,  
555 Wisthaler, A., Mikoviny, T., Jimenez, J. L., Campuzano-Jost, P., Day, D. A., Hu, W., Ryerson, T. B., Pollack, I.  
556 B., Peischl, J., Anderson, B. E., Ziemba, L. D., Blake, D. R., Meinardi, S., and Diskin, G.: Airborne measurements  
557 of organosulfates over the continental US, *Journal of Geophysical Research-Atmospheres*, 120, 2990-3005, 2015.
- 558 Ma, Y., Xu, X., Song, W., Geng, F., and Wang, L.: Seasonal and diurnal variations of particulate organosulfates in  
559 urban Shanghai, China, *Atmospheric Environment*, 85, 152-160, 2014.
- 560 Malm, W. C., and Kreidenweis, S. M.: The effects of models of aerosol hygroscopicity on the apportionment of  
561 extinction, *Atmos. Environ.*, 31, 1965-1976, 1997.
- 562 Marcolli, C., and Krieger, U. K.: Phase changes during hygroscopic cycles of mixed organic/inorganic model systems  
563 of tropospheric aerosols, *J. Phys. Chem. A*, 110, 1881-1893, 2006.
- 564 McNeill, V. F., Woo, J. L., Kim, D. D., Schwier, A. N., Wannell, N. J., Sumner, A. J., and Barakat, J. M.: Aqueous-  
565 Phase Secondary Organic Aerosol and Organosulfate Formation in Atmospheric Aerosols: A Modeling Study,  
566 *Environmental Science & Technology*, 46, 8075-8081, 2012.
- 567 Moise, T., Flores, J. M., and Rudich, Y.: Optical properties of secondary organic aerosols and their changes by  
568 chemical processes, *Chem Rev*, 115, 4400-4439, 2015.
- 569 Moore, R. H., Nenes, A., and Medina, J.: Scanning Mobility CCN Analysis-A Method for Fast Measurements of Size-  
570 Resolved CCN Distributions and Activation Kinetics, *Aerosol Science and Technology*, 44, 861-871, 2010.
- 571 Noziere, B., Kaberer, M., Claeys, M., Allan, J., D'Anna, B., Decesari, S., Finessi, E., Glasius, M., Grgic, I., Hamilton,  
572 J. F., Hoffmann, T., Iinuma, Y., Jaoui, M., Kahno, A., Kampf, C. J., Kourtchev, I., Maenhaut, W., Marsden, N.,  
573 Saarikoski, S., Schnelle-Kreis, J., Surratt, J. D., Szidat, S., Szmigielski, R., and Wisthaler, A.: The Molecular  
574 Identification of Organic Compounds in the Atmosphere: State of the Art and Challenges, *Chemical Reviews*,  
575 115, 3919-3983, 2015.
- 576 Pöschl, U.: Atmospheric aerosols: composition, transformation, climate and health effects, *Angewandte Chemie*  
577 *International Edition*, 44, 7520-7540, 2005.
- 578 Peng, C., Jing, B., Guo, Y. C., Zhang, Y. H., and Ge, M. F.: Hygroscopic Behavior of Multicomponent Aerosols  
579 Involving NaCl and Dicarboxylic Acids, *The journal of physical chemistry. A*, 120, 1029-1038, 2016.
- 580 Petters, M. D., and Kreidenweis, S. M.: A single parameter representation of hygroscopic growth and cloud  
581 condensation nucleus activity, *Atmospheric Chemistry And Physics*, 7, 1961-1971, 2007.
- 582 Petters, M. D., and Kreidenweis, S. M.: A single parameter representation of hygroscopic growth and cloud  
583 condensation nucleus activity - Part 2: Including solubility, *Atmospheric Chemistry and Physics*, 8, 6273-6279,  
584 2008.
- 585 Petters, M. D., Wex, H., Carrico, C. M., Hallbauer, E., Massling, A., McMeeking, G. R., Poulain, L., Wu, Z.,  
586 Kreidenweis, S. M., and Stratmann, F.: Towards closing the gap between hygroscopic growth and activation for  
587 secondary organic aerosol - Part 2: Theoretical approaches, *Atmospheric Chemistry and Physics*, 9, 3999-4009,  
588 2009.
- 589 Petters, M. D., and Kreidenweis, S. M.: A single parameter representation of hygroscopic growth and cloud  
590 condensation nucleus activity - Part 3: Including surfactant partitioning, *Atmospheric Chemistry and Physics*, 13,  
591 1081-1091, 2013.
- 592 Pitzer, K. S., and Mayorga, G.: Thermodynamics of electrolytes. 2. Activity and osmotic coefficients for strong  
593 electrolytes with one or both ions univalent, *Journal of Physical Chemistry*, 77, 2300-2308, 1973.
- 594 Prenni, A.: Water uptake of internally mixed particles containing ammonium sulfate and dicarboxylic acids, *Atmos.*  
595 *Environ.*, 37, 4243-4251, 2003.
- 596 Riva, M., Chen, Y., Zhang, Y., Lei, Z., Olson, N. E., Boyer, H. C., Narayan, S., Yee, L. D., Green, H. S., Cui, T.,  
597 Zhang, Z., Baumann, K., Fort, M., Edgerton, E., Budisulistiorini, S. H., Rose, C. A., Ribeiro, I. O., RL, E. O.,  
598 Dos Santos, E. O., Machado, C. M. D., Szopa, S., Zhao, Y., Alves, E. G., de Sa, S. S., Hu, W., Knipping, E. M.,  
599 Shaw, S. L., Duvoisin Junior, S., de Souza, R. A. F., Palm, B. B., Jimenez, J. L., Glasius, M., Goldstein, A. H.,  
600 Pye, H. O. T., Gold, A., Turpin, B. J., Vizuete, W., Martin, S. T., Thornton, J. A., Dutcher, C. S., Ault, A. P., and  
601 Surratt, J. D.: Increasing Isoprene Epoxydiol-to-Inorganic Sulfate Aerosol Ratio Results in Extensive Conversion  
602 of Inorganic Sulfate to Organosulfur Forms: Implications for Aerosol Physicochemical Properties, *Environ Sci*  
603 *Technol*, 53, 8682-8694, 2019.
- 604 Roberts, G. C., and Nenes, A.: A continuous-flow streamwise thermal-gradient CCN chamber for atmospheric  
605 measurements, *Aerosol Science and Technology*, 39, 206-221, 2005.
- 606 Shrivastava, M., Cappa, C. D., Fan, J., Goldstein, A. H., Guenther, A. B., Jimenez, J. L., Kuang, C., Laskin, A., Martin,  
607 S. T., Ng, N. L., Petaja, T., Pierce, J. R., Rasch, P. J., Roldin, P., Seinfeld, J. H., Shilling, J., Smith, J. N., Thornton,  
608 J. A., Volkamer, R., Wang, J., Worsnop, D. R., Zaveri, R. A., Zelenyuk, A., and Zhang, Q.: Recent advances in



- 609 understanding secondary organic aerosol: Implications for global climate forcing, *Reviews of Geophysics*, 55,  
610 509-559, 2017.
- 611 Staudt, S., Kundu, S., Lehmler, H.-J., He, X., Cui, T., Lin, Y.-H., Kristensen, K., Glasius, M., Zhang, X., Weber, R.  
612 J., Surratt, J. D., and Stone, E. A.: Aromatic organosulfates in atmospheric aerosols: Synthesis, characterization,  
613 and abundance, *Atmospheric Environment*, 94, 366-373, 2014.
- 614 Stokes, R. H., and Robinson, R. A.: INTERACTIONS IN AQUEOUS NONELECTROLYTE SOLUTIONS .I.  
615 SOLUTE-SOLVENT EQUILIBRIA, *Journal of Physical Chemistry*, 70, 2126-&, 1966.
- 616 Surratt, J. D., Gomez-Gonzalez, Y., Chan, A. W. H., Vermeylen, R., Shahgholi, M., Kleindienst, T. E., Edney, E. O.,  
617 Offenberg, J. H., Lewandowski, M., Jaoui, M., Maenhaut, W., Claeys, M., Flagan, R. C., and Seinfeld, J. H.:  
618 Organosulfate formation in biogenic secondary organic aerosol, *Journal of Physical Chemistry A*, 112, 8345-  
619 8378, 2008.
- 620 Svenningsson, B., Rissler, J., Swietlicki, E., Mircea, M., Bilde, M., Facchini, M. C., Decesari, S., Fuzzi, S., Zhou, J.,  
621 Monster, J., and Rosenorn, T.: Hygroscopic growth and critical supersaturations for mixed aerosol particles of  
622 inorganic and organic compounds of atmospheric relevance, *Atmospheric Chemistry and Physics*, 6, 1937-1952,  
623 2006.
- 624 Tang, M., Cziczo, D. J., and Grassian, V. H.: Interactions of Water with Mineral Dust Aerosol: Water Adsorption,  
625 Hygroscopicity, Cloud Condensation, and Ice Nucleation, *Chemical Reviews*, 116, 4205-4259, 2016.
- 626 Tang, M., Chan, C. K., Li, Y. J., Su, H., Ma, Q., Wu, Z., Zhang, G., Wang, Z., Ge, M., Hu, M., He, H., and Wang, X.:  
627 A review of experimental techniques for aerosol hygroscopicity studies, *Atmospheric Chemistry and Physics*, 19,  
628 12631-12686, 2019a.
- 629 Tang, M., Gu, W., Ma, Q., Li, Y. J., Zhong, C., Li, S., Yin, X., Huang, R.-J., He, H., and Wang, X.: Water adsorption  
630 and hygroscopic growth of six anemophilous pollen species: the effect of temperature, *Atmospheric Chemistry  
631 and Physics*, 19, 2247-2258, 2019b.
- 632 Tolocka, M. P., and Turpin, B.: Contribution of Organosulfur Compounds to Organic Aerosol Mass, *Environmental  
633 Science & Technology*, 46, 7978-7983, 2012.
- 634 Wang, K., Zhang, Y., Huang, R.-J., Wang, M., Ni, H., Kampf, C. J., Cheng, Y., Bilde, M., Glasius, M., and Hoffmann,  
635 T.: Molecular Characterization and Source Identification of Atmospheric Particulate Organosulfates Using  
636 Ultrahigh Resolution Mass Spectrometry, *Environmental Science & Technology*, 53, 6192-6202, 2019a.
- 637 Wang, Y., Hu, M., Guo, S., Wang, Y., Zheng, J., Yang, Y., Zhu, W., Tang, R., Li, X., Liu, Y., Le Breton, M., Du, Z.,  
638 Shang, D., Wu, Y., Wu, Z., Song, Y., Lou, S., Hallquist, M., and Yu, J.: The secondary formation of  
639 organosulfates under interactions between biogenic emissions and anthropogenic pollutants in summer in Beijing,  
640 *Atmospheric Chemistry and Physics*, 18, 10693-10713, 2018.
- 641 Wang, Y., Ma, Y., Li, X., Kuang, B. Y., Huang, C., Tong, R., and Yu, J. Z.: Monoterpene and Sesquiterpene alpha-  
642 Hydroxy Organosulfates: Synthesis, MS/MS Characteristics, and Ambient Presence, *Environ Sci Technol*, 2019b.
- 643 Wang, Y., Hu, M., Wang, Y.-C., Li, X., Fang, X., Tang, R., Lu, S., Wu, Y., Guo, S., Wu, Z., Hallquist, M., and Yu,  
644 J. Z.: Comparative Study of Particulate Organosulfates in Contrasting Atmospheric Environments: Field  
645 Evidence for the Significant Influence of Anthropogenic Sulfate and NO<sub>x</sub>, *Environmental Science & Technology  
646 Letters*, 2020.
- 647 Wex, H., Petters, M., Carrico, C., Hallbauer, E., Massling, A., McMeeking, G., Poulain, L., Wu, Z., Kreidenweis, S.,  
648 and Stratmann, F.: Towards closing the gap between hygroscopic growth and activation for secondary organic  
649 aerosol: Part 1—Evidence from measurements, *Atmospheric Chemistry and Physics*, 9, 3987-3997, 2009.
- 650 Wexler, A. S., and Clegg, S. L.: Atmospheric aerosol models for systems including the ions H<sup>+</sup>, NH<sub>4</sub><sup>+</sup>, Na<sup>+</sup>, SO<sub>4</sub><sup>2-</sup>,  
651 NO<sub>3</sub><sup>-</sup>, Cl<sup>-</sup>, Br<sup>-</sup>, and H<sub>2</sub>O, *J. Geophys. Res.*, 107, 2002.
- 652 Wise, M. E., Surratt, J. D., Curtis, D. B., Shilling, J. E., and Tolbert, M. A.: Hygroscopic growth of ammonium  
653 sulfate/dicarboxylic acids, *J. Geophys. Res.*, 108, 2003.
- 654 Wu, Z. J., Nowak, A., Poulain, L., Herrmann, H., and Wiedensohler, A.: Hygroscopic behavior of atmospherically  
655 relevant water-soluble carboxylic salts and their influence on the water uptake of ammonium sulfate,  
656 *Atmospheric Chemistry and Physics*, 11, 12617-12626, 2011.
- 657 Zardini, A. A., Sjogren, S., Marcolli, C., Krieger, U. K., Gysel, M., Weingartner, E., Baltensperger, U., and Peter, T.:  
658 A combined particle trap/HTDMA hygroscopicity study of mixed inorganic/organic aerosol particles, *Atmos.  
659 Chem. Phys.*, 8, 5589-5601, 2008.
- 660 Zhang, Y.-Q., Chen, D.-H., Ding, X., Li, J., Zhang, T., Wang, J.-Q., Cheng, Q., Jiang, H., Song, W., Ou, Y.-B., Ye,  
661 P.-L., Zhang, G., and Wang, X.-M.: Impact of anthropogenic emissions on biogenic secondary organic aerosol:  
662 observation in the Pearl River Delta, southern China, *Atmospheric Chemistry and Physics*, 19, 14403-14415,  
663 2019.
- 664